DOI: 10.1007/s12541-011-0111-y

Development of a New Gerotor for Oil Pumps with Multiple Profiles

Sung-Yuen Jung[1], Jun-Ho Bae[2], Moon-Saeng Kim[2] and Chul Kim[1,#]

1 Research Institute of Mechanical Technology, Pusan National University, San30, Jangjeon-dong, Geumjeong-gu, Busan, South Korea, 609-735
2 School of Mechanical Engineering, Pusan National University, San30, Jangjeon-dong, Geumjeong-gu, Busan, South Korea, 609-735
Corresponding Author / E-mail: chulki@pusan.ac.kr, TEL: +82-51-510-2489, FAX: +82-51-512-9835

KEYWORDS: Combined profile lobe, Internal lobe pumps, Flow rate, Irregularity, Taguchi method

The use of an internal lobe pump is suitable for enhancing the oil hydraulics of machine tools, automotive engines, compressors, constructions and various other applications. In particular, the pump is an essential machine element for supplying lubricants in an automotive engine. The subject of this paper is the theoretical analysis of an internal lobe pump whose main components are inner and outer rotors; the outer rotor is characterized by a lobe with multiple profile shapes (ellipse 1, involute, and ellipse 2), while the profile of the inner rotor is determined as a function of the profile of the outer rotor. Further, the design of the outer rotor depends on new applications and it eliminates the carryover phenomenon. The system suggested in this study generates a new lobe profile and automatically calculates the flow rate and flow rate irregularity according to the generated lobe profile. In this study, the Taguchi method is used to determine the optimal rotor shapes and design parameters of the pump performance. The results obtained by the analysis enable the designer and manufacturer of oil pumps to achieve higher efficiency.

Manuscript received: January 11, 2011 / Accepted: April 10, 2011

1. Introduction

Internal lobe pumps are widely used as lubricant sources or as hydraulic sources of engine lubrication for automatic transmission, since the noise generated by the inner and outer rotors in these pumps is lower than that generated by other types of pumps. Colbourne[1] obtained the coordinates of the inner rotor lobes by simulating the contact between inner and outer rotors and calculating the area of the chamber enclosed by the lobe curve. Saegusa et al.[2] obtained the trajectory measurements of the arc centers and lobes of the outer rotor by fixing the inner rotor and rotating the outer rotors, and they derived the formula for obtaining the lobes of the inner rotor from the engagement characteristics of the inner and outer rotors. Recently, Tsay[3,4] described the process of obtaining the lobes of the inner rotor by simulating the cutting process. Lee et al.[5] analyzed the operational characteristics, while Mimmi et al.[6] compared the flow rates and flow rate irregularity for involute gear pumps with those for lobe pumps. Kim et al.[7,8] observed the change in contact stress with changes in gerotor design variables, and studied on other component related to the pump. Kim et al.[9-12] proposed a new method for deriving lobe equations for the trochoid lobe of the gerotor pumps for the case in which the profile of the outer rotor is a circle or a combination of an ellipse and an involute, and they developed an integrated system for automatically obtaining the trajectories of the inner rotor, outer rotor and contact points, for simulating the rotation, and for obtaining the flow rate, flow rate irregularity, and other parameters. An ellipse-involute shape is a shape in which the involute is inserted in a specific part of the ellipse. Therefore, the discontinuity of the curves occurs at the point of intersection of the ellipse and the involute, and this causes the problems of increased noise and decreased durability.

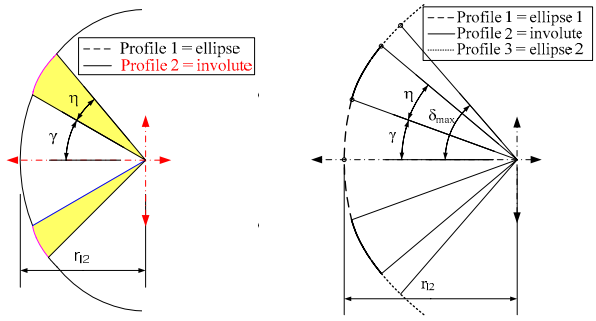

(a) Lobe profile of ellipse-involute (b) Lobe profile of ellipse1-involute-ellipse 2

Fig. 1 Comparison between the previous lobe profile and new lobe profile

© KSPE and Springer 2011

In this study, to prevent the generation of the discontinuity point by the combination of the ellipse and involute, a new design method based on the use of the lobe shape of the outer rotor with multiple profiles (ellipse 1, involute, and ellipse 2) is proposed. The constitutive equation for the point of intersection of the inner and outer rotors is established; this equation includes the design parameters. Further, the outer rotor is designed such that the carryover phenomenon is eliminated. This is achieved by using the designed shapes of the inner and outer rotors. The optimal design of the inner and outer rotors is obtained by the Taguchi method based on the flow rate and flow rate irregularity of the pump performance parameters.

2. Design of Inner Rotor using point of Intersection of Inner and Outer Rotors[6]

The number of outer rotor lobes, z_2 is greater than the number of inner rotor lobes, z_1 by one and the pitch circle radii of the inner and outer rotors are expressed as follows.

$$z_2 = z_1 + 1, \quad r_1 = ez_1, r_2 = ez_2 \tag{1}$$

When the lobe profile of the outer rotor is rotated by α^i, the line connecting the point of intersection of the inner and outer rotors, A', to the pitch point, P, becomes the normal line of the inner rotor. For the case in which the lobe profile of the outer rotor is a circle, the center point of the lobe profile lies on the line connecting the point of intersection to the pitch point. Therefore, the point of intersection, A' is given by Eq. (2).

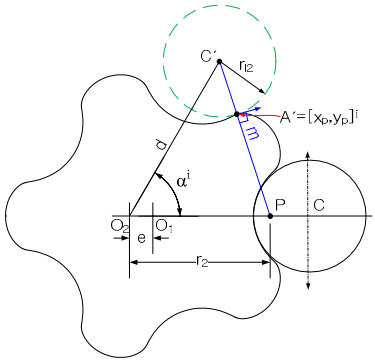

Fig. 2 Tracing the conjugated profile tracing for circle

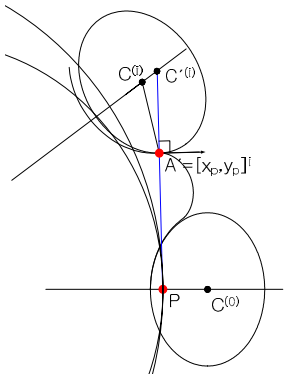

Fig. 3 Tracing the conjugated profile tracing for ellipse

$$A = \begin{Bmatrix} x_p(\alpha^i) \\ y_p(\alpha^i) \end{Bmatrix} = \begin{pmatrix} d\cos\alpha^i - \frac{r_{l2}}{m}\left(d\cos\alpha^i - r_2\right) \\ d\sin\alpha^i - \frac{r_{l2}}{m} d\sin\alpha^i \end{pmatrix} \tag{2}$$

with $m = \sqrt{r_2^2 + d^2 - 2r_2 d\cos\alpha^i}$

However, when the lobe profile of the outer rotor is not a circle, the center point of the lobe profile dose not lie on the line connecting the intersection point to the pitch point.

In this study, the constitutive equation for the lobe profile with multiple profiles (ellipse 1, involute, and ellipse 2) is derived by the Newton-Rahpson method.

2.1 Combination of Lobe with Multiple Profiles

The lobe shape of the outer rotor with multiple profiles (ellipse 1, involute, and ellipse 2) is shown in Fig. 4. The points at which each part begins and ends are given by Eq. (3). For the lobe shape of the outer rotor with multiple profiles (ellipse 1, involute, and ellipse 2), first, ellipse 1 is determined; the design parameters are the distance from the center of the outer rotor to the center of the ellipse, d, the major-minor axis ratio of the ellipse, k and the length of the minor axis of the ellipse, r_{12}. Then, the involute is determined by using ellipse 1, and the part of the ellipse that contains the involute is that from point P_{11} at the starting angle ($\delta_{ellipse}$= γ) to point P_{12} at the ending angle ($\delta_{ellipse}$= γ+η). The parameters of the involute are shown in Fig. 5. In ellipse 1, the length of the line connecting the point at the starting angle, P_{21}, to the point at the ending angle, P_{22} is L_e, the gradient of the line is L_{grad}, the involute that is contained in the part of the ellipse is L_i, and the gradient of L_i is equal to L_{grad}.

$$\begin{aligned} P_{ij},\ i &= profile\ number \\ j &= boundary\ point \end{aligned} \tag{3}$$

The magnitude of the involute is determined by using Eq. (4). The $factor_{rb}$ is the scale factor of the involute with the radius, r_b, of the base circle. P_{13} is equal to P_{22} when $factor_{rb} = 1$, the curvature of the involute becomes greater than that of ellipse 1 when $factor_{rb} > 1$, and the curvature of the involute becomes less than that of the ellipse 1 when $factor_{rb} < 1$.

$$r_{b,\neq w} = factor_{rb} \times \left(\frac{L_e}{L_i}\right) \tag{4}$$

After determining the profile for the involute, the coordinate transformation of the profile is performed by using Eq. (5).

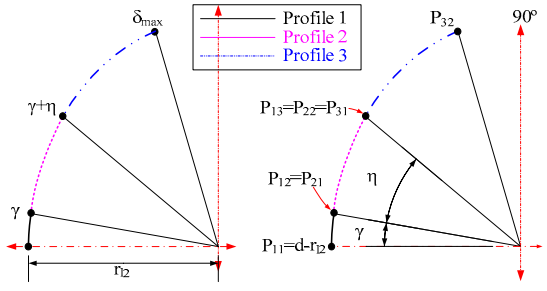

Fig. 4 Tracing the conjugated lobe profile for new rotor

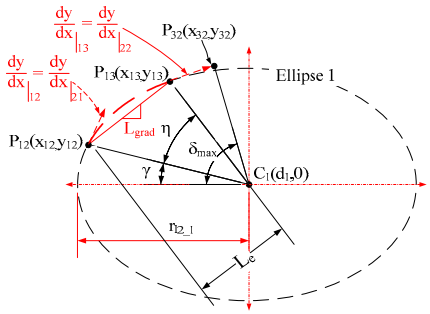

(a) Conjugated profile for ellipse

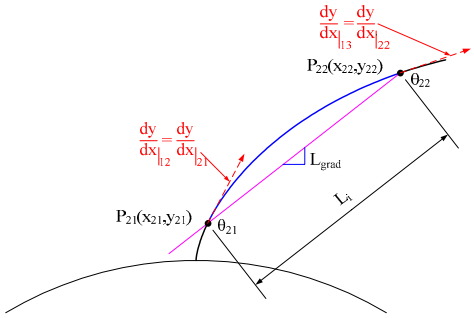

(b) Conjugated profile for involute

Fig. 5 Conjugated lobe profile for ellipse 1 and involute

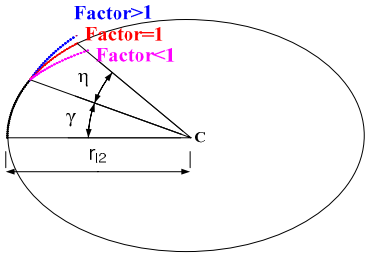

Fig. 6 Scale factor of involute for lobe profile

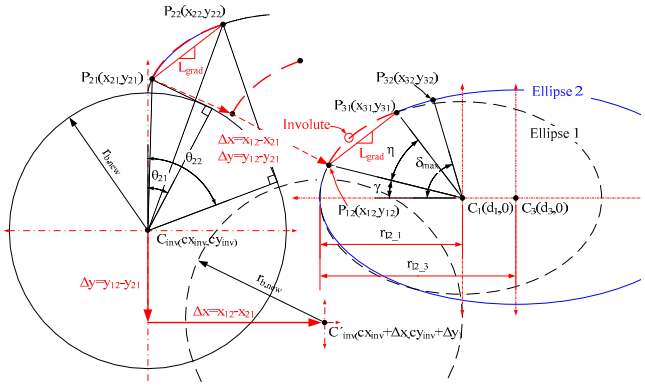

Fig. 7 Lobe profile for combination three different curvatures

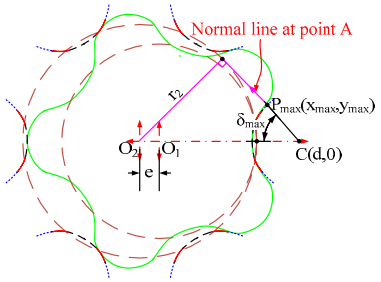

Fig. 8 Determining δ_{max}

$$C'_{inv} = \begin{pmatrix} cx_{inv} + \Delta x \\ cy_{inv} + \Delta y \end{pmatrix}, \begin{pmatrix} \Delta x \\ \Delta y \end{pmatrix} = \begin{pmatrix} x_{12} - x_{21} \\ y_{12} - y_{21} \end{pmatrix} \tag{5}$$

The trajectory of the involute after the coordinate transformation is given by Eq. (6).

$$\begin{aligned} x_{inv,new} &= r_{b,new}(\sin\theta_{inv} - \theta_{inv}\cos\theta_{inv}) + \Delta x \\ y_{inv,new} &= r_{b,new}(\cos\theta_{inv} - \theta_{inv}\sin\theta_{inv}) + \Delta y \end{aligned} \tag{6}$$

The lobe profile of ellipse 2 combined with the involute is determined by using Eqs. (7)-(10). This determination is based on the fact that the gradient of the tangent of the involute is equal to that of ellipse 2 at the point at which the involute ends, P_{22}, and the fact that the center of ellipse 2 lies on the x-axis.

$$\frac{dy}{dx(P_{31})_{ellipse}} = \frac{1}{k_3}\cot\theta_{31},\ \theta_{31} = \tan^{-1}(\tan\theta_{22}) \tag{7}$$

$$k_3 = \sqrt{\cot\theta_{22}\frac{y_{22}}{x_{22}}} \tag{8}$$

$$r_{l2,3} = \frac{x_{22}}{\cos\theta_{31}} \tag{9}$$

$$d_3 = r_{l2,3} \times \cos\theta_{31} + x_{22} \tag{10}$$

Eq. (11) is the equation of the normal line on the ellipse with $\theta = \theta_{max}$.

$$y = -\frac{\tan\theta_{max}}{k}(x - d + r_{l2}\cos\theta_{max}) + kr_{l2}\sin\theta_{max} \tag{11}$$

The distance from the normal line to point O_2 is equal to r_2 and is calculated by using Eq. (12). The real root, θ_{max}, is calculated from Eq. (12) by using the solution of Ferrari, and δ_{max} is calculated by substituting θ_{max} into Eq. (13).

$$r_2 = \frac{\left|d\tan\theta_{max} - r_{l2}\sin\theta_{max} + k^2 r_{l2}\sin\theta_{max}\right|}{\sqrt{\tan^2\theta_{max} + k^2}} \tag{12}$$

$$\delta_{max} = \tan^{-1}(k\tan\theta_{max}) \tag{13}$$

2.2 Constitutive Equation for Contact Point derived by Newton-Rahpson Method

When the lobe profile of the outer rotor is an ellipse or involute and not a circle, the normal line at a contact point is not directed toward the center of the ellipse or involute. Therefore, θ_{cir} or θ_{inv} is calculated by using Newton-Rahpson method for satisfying Eq. (14), (15) and connecting from the point, P' which is the pitch point, P rotated counter clockwise as α to the point on the involute profile as shown in Fig. 9.

The gradient of the tangent line is calculated by using Eq. (15), and that of the normal line is calculated by using Eq. (16) that is related to the parametric equation of the circle, Eq. (14).

$$\begin{pmatrix} x \\ y \end{pmatrix} = \begin{pmatrix} d - r_{l2}\cos\theta \\ -kr_{l2}\sin\theta \end{pmatrix} \tag{14}$$

$$\frac{dy}{dx} = \frac{dy}{d\theta}\frac{d\theta}{dx} = \frac{-kr_{l2}\cos\theta}{r_{l2}\sin\theta} = -k\cot\theta \tag{15}$$

$$-\frac{1}{f'(\theta)} = -(-k\cot\theta)^{-1} = \frac{1}{k}\tan\theta \tag{16}$$

The coordinates of point A and point P are shown in Eq. (17) and Eq. (18). Eq. (19) is established because the gradient of AP is equal to that of AC'.

$$A = (d - r_{l2}\cos\theta,\ -kr_{l2}\sin\theta) \tag{17}$$

$$P = (r_2\cos\alpha,\ -r_2\sin\alpha) \tag{18}$$

$$\frac{-kr_{l2}\sin\theta + r_2\sin\alpha}{d - r_{l2}\cos\theta - r_2\cos\alpha} = \frac{1}{k}\tan\theta \tag{19}$$

The Eq. (20) is obtained by substituting θ which is derived by using the Newton-Rahpson method in Eq. (19) into Eq. (17).

$$(k^2-1)r_{l2}\sin\theta - (r_2\cos\alpha - d)\tan\theta = kr_2\sin\alpha \tag{20}$$

The function $f(\theta)$ and $f'(\theta)$ of the parameter θ with the given α are defined by Eq. (21) and Eq. (22).

$$f(\theta) = (k^2-1)r_{l2}\sin\theta - (r_2\cos\alpha - d)\tan\theta - kr_2\sin\alpha \tag{21}$$

$$f'(\theta) = (k^2-1)r_{l2}\cos\theta - (r_2\cos\alpha - d)\sec^2\theta \tag{22}$$

The coordinate of point A' is that of point A rotated counter clockwise by α and is calculated by using Eq. (23).

$$A' = \begin{pmatrix} x_c \\ y_c \end{pmatrix} = \begin{pmatrix} \cos\alpha & -\sin\alpha \\ \sin\alpha & \cos\alpha \end{pmatrix}\begin{pmatrix} d - r_{l2}\cos\theta \\ -kr_{l2}\sin\theta \end{pmatrix} = \begin{pmatrix} \cos\alpha(d - r_{l2}\cos\theta) + kr_{l2}\sin\alpha\sin\theta \\ \sin\alpha(d - r_{l2}\cos\theta) - kr_{l2}\cos\alpha\sin\theta \end{pmatrix} \tag{23}$$

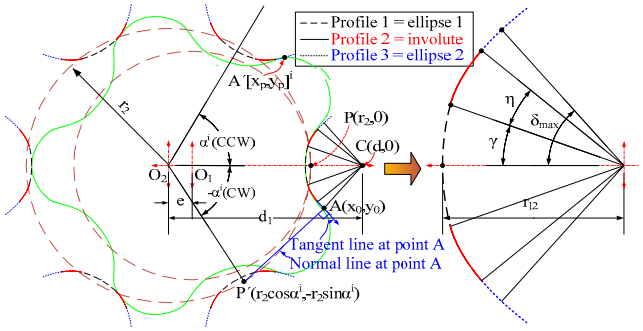

Fig. 9 Conjugated profile tracing for deriving the new rotor point equation

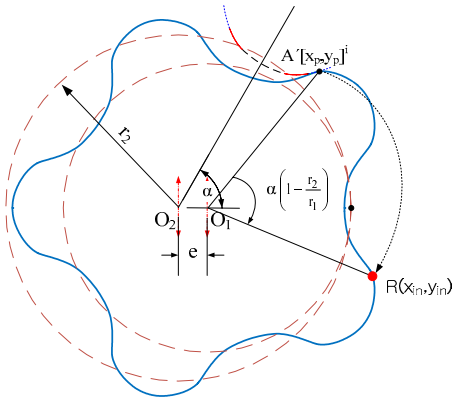

Fig. 10 Profile tracing for tri-choid shape

2.3 Design of Inner Rotor Using Contact Point

The point of the trajectory, R(x_{in}, y_{in}) is derived from the contact point, A, by Eq. (24).

$$\begin{pmatrix} x_{in} \\ y_{in} \end{pmatrix} = \begin{pmatrix} \cos\alpha' & -\sin\alpha' \\ \sin\alpha' & \cos\alpha \end{pmatrix}\begin{pmatrix} x_c - e \\ y_c \end{pmatrix} + \begin{pmatrix} e \\ 0 \end{pmatrix} \quad \text{with} \quad \alpha' = \alpha\left(1 - \frac{r_2}{r_1}\right) \tag{24}$$

3. Design of Outer Rotor for Eliminating Carryover Phenomenon

When the inner rotor is designed using the point of contact between the inner and outer rotor, the carryover phenomenon is observed, as shown in Fig. 11. When the fluid is transported from a high-pressure port to a low-pressure port, the volume loss occurs because of the geometric error, and the volume efficiency of the pump is decreased.

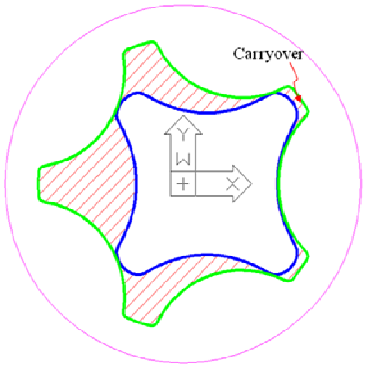

Fig. 11 Traditional design of a gerotor

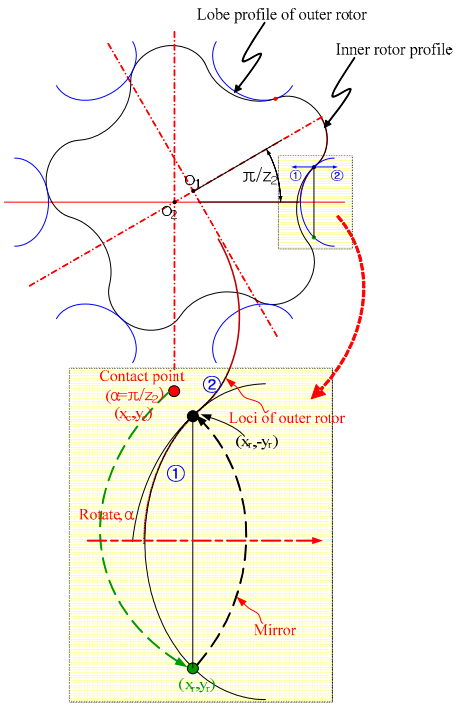

Fig. 12 New design method for the outer rotor

To eliminate the carryover phenomenon, the outer rotor is designed by using the curvature profile of the inner rotor. When the radius of curvature of the inner rotor is maximum, the inner rotor is rotated by the angle α from the center of the outer rotor; α is given by Eq. (25), and the tooth number of the outer rotor, Z_2, is shown in Fig. 12. At this stage, the profile of the inner rotor is perfectly matched to the dedendum of the outer rotor.

$$\alpha = \frac{\pi}{z_2} \rightarrow \text{contact point} : (x_c, y_c) \tag{25}$$

In this study, the dedendum of the outer rotor is determined by the input lobe profile, and the addendum that results in the carryover phenomenon is determined by using the lobe profile of the outer rotor. An example of the profile design of the outer rotor is shown in Fig. 12. A part of the dedendum, ①, consists of the lobe profile of the outer rotor, and a part of the addendum, ②, consists of the profile rotated by the angle given by Eq. (25); the latter profile is that of the inner rotor rotated from the center of the outer rotor. The boundary point of ① and ② is given by Eq. (26).

$$\begin{pmatrix} x_r \\ -y_r \end{pmatrix} = \begin{pmatrix} \cos\frac{\pi}{z_2} & -\sin\frac{\pi}{z_2} \\ \sin\frac{\pi}{z_2} & \cos\frac{\pi}{z_2} \end{pmatrix} \begin{pmatrix} x_c \\ -y_c \end{pmatrix} \tag{26}$$

The lobe profile of the outer rotor in Fig. 13 is designed by the new design method proposed in this study, and the carryover phenomenon is eliminated.

4. Application and Considerations

The Taguchi method is implemented for obtaining the optimal design of the lobe profile with the combination of ellipse 1, involute and ellipse 2. The variable parameters and the level values of the lobe profile are listed in Table 1.

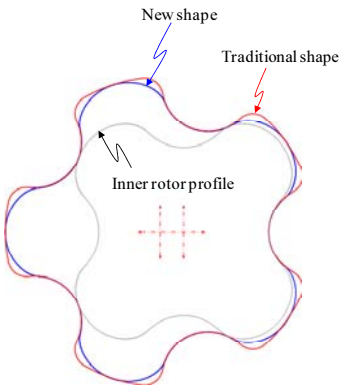

Fig. 13 Schematic illustration of the outer rotor designed by using the new method

Table 1 Design parameters and level values of lobe profiles

Design parameter	Level value				
e	1.170	1.175	1.180	1.185	1.190
d	12.00	12.02	12.04	12.06	12.08
k	1.08	1.10	1.12	1.14	1.16
γ	52	54	56	58	60
η	20.00	21.25	22.50	23.75	25.00
f	0.90	1.05	1.20	1.35	1.50

The orthogonal array of the variable parameters is presented in Table 1. The lobe profile is designed by using the automatic design program, and the results of the analysis of the flow rate and flow rate irregularity are shown in Fig. 14. The eccentricity of the parameters, e, has the strongest effect on the flow rate, and the flow rate increases with the eccentricity, as shown in Fig. 14(a). The analysis results in Fig. 14(b) indicate that as the distance between the center of the outer rotor and the center of lobe profile, d, increases and the eccentricity, e, increases, the flow rate irregularity decreases.

The four cases in which the optimal parameters have the strongest effect on the flow rate and flow rate irregularity are listed in Table 2.

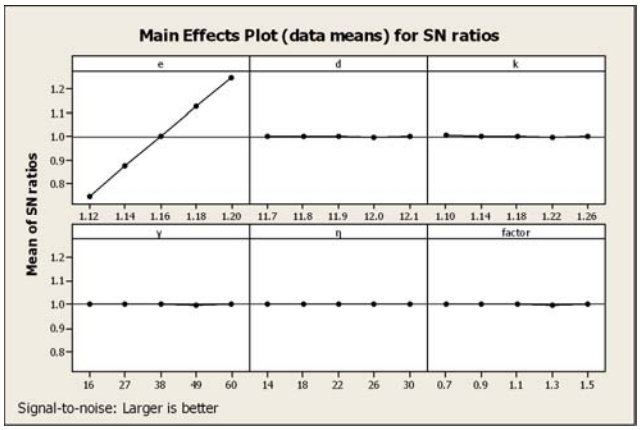

(a) SN ratio for the flow rate

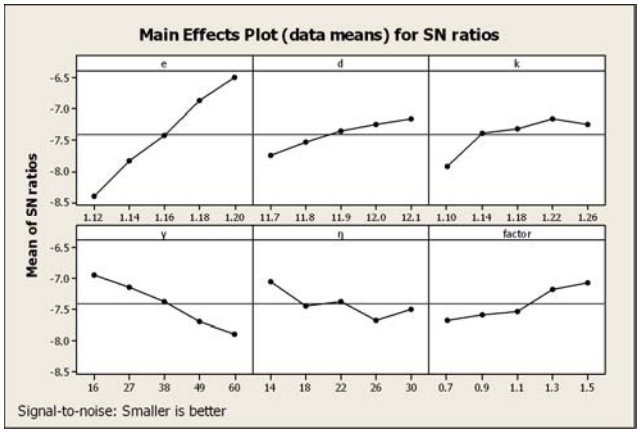

(b) SN ratio for the flow rate irregularity

Fig. 14 Analysis of flow rate and flow rate irregularity

Table 2 Optimal design parameters of lobe profiles

Case	e	d	k	r_{12}	γ	η	f	q	i
Rotor 1-1	1.16	12.08	1.163	2.42	56.7°	25°	20	0.972	97.22
Rotor 1-2	1.16	12	1.16	2.34	60°	20°	20	0.972	97.21
Rotor 1-3	1.18	12.08	1.138	2.46	53°	20°	0.9	0.93	97.69
Rotor 1-4	1.18	12.08	1.12	2.46	60°	25°	1.2	0.977	97.66

Table 3 Test results of variable profiles

Case		13V 450kPa		8V 450kPa	
		Flow rate	Efficiency	Flow rate	Efficiency
Rotor 1-1	1st test (10min.)	198.4	24.7	84.3	12.7
	1st test (20hr.)	188.1	26.0	74.9	12.0
	2st test (10min.)	207.7	28.9	80.0	13.0
	2st test (20hr.)	196.6	28.4	68.7	11.2
	3st test (10min.)	204.8	26.5	79.7	11.8
	3st test (20hr.)	196.3	27.0	81.3	13.3
	Average (Tests for 10min.)	203.6	26.7	81.3	12.5
	Average (Tests for 20hr.)	193.7	27.1	75.0	12.2
Rotor 1-2	1st test (10min.)	200.0	26.4	80.4	12.6
	1st test (20hr.)	204.7	26.3	79.2	12.6
	2st test (10min.)	205.9	25.9	86.4	13.0
	2st test (20hr.)	190.6	25.3	78.3	12.2
	3st test (10min.)	198.5	25.5	84.2	13.3
	3st test (20hr.)	175.8	21.0	67.8	10.0
	Average (Tests for 10min.)	201.5	25.9	83.7	12.9
	Average (Tests for 20hr.)	187.0	24.2	75.1	11.6
Rotor 1-3	1st test (10min.)	210.5	23.1	88.0	11.4
	1st test (20hr.)	200.5	23.7	86.3	11.9
	2st test (10min.)	224.6	26.1	85.3	10.1
	2st test (20hr.)	222.7	27.4	81.4	9.8
	3st test (10min.)	219.2	26.3	97.0	13.5
	3st test (20hr.)	206.7	26.3	99.9	15.6
	Average (Tests for 10min.)	218.1	25.2	90.1	11.7
	Average (Tests for 20hr.)	210.0	25.8	89.2	12.4
Rotor 1-4	1st test (10min.)	215.2	26.1	91.7	13.0
	1st test (20hr.)	206.8	26.7	91.6	14.4
	2st test (10min.)	214.5	24.6	91.3	12.1
	2st test (20hr.)	222.3	26.8	93.5	12.6
	3st test (10min.)	216.2	26.3	93.8	13.5
	3st test (20hr.)	205.9	25.2	95.7	14.6
	Average (Tests for 10min.)	215.3	25.7	92.3	12.9
	Average (Tests for 20hr.)	211.7	26.2	93.6	13.9

(a) Ellipse-involute gerotor (b) Ellipse1-involute-ellipse2 gerotor

Fig. 15 Previous and new gerotors

Table 4 Comparison of results for the previous and new gerotors

Product	z_2	e	d	r_{i2}	k	γ	η	*factor*	Flow rate (*l/hr*)	Irregularity (%)
(a) Ellipse-involute	10	1.15	11.93	2.25	1.21	0°	20°	.	198.7	2.29
(b) Ellips1-involute-ellipse2	10	1.18	12.08	2.46	1.12	60°	25°	1.2	210.0	2.27

The test results for the four prototypes correspnding to the cases in Table 2 are listed in Table 3. In the case Rotor 1-4, the optimal design is achieved for 20 hours flow rate and efficiency. A comparison with the ellipse-involute profile and the ellipse 1-involute-ellipse 2 profile that has been proposed in this study is presented in Table 4, and the prototypes of gerotors with the above mentioned profiles are shown in Fig. 15.

The flow rate and flow rate irregularity in the case Rotor 1-4 are better than those in the case of previous design, namely, the ellipse-involute rotor.

5. Conclusions

In this study, the constitutive equation for rotors is established by the geometric and kinematic analysis of an outer rotor that has a lobe shape with multiple profiles (ellipse 1, involute, and ellipse 2). The Taguchi method is implemented for obtaining the optimal design of the rotor with the maximum flow rate and minimum flow rate irregularity. The results obtained are summarized below.

1. A new design of gerotor is proposed by using the outer rotor that has a lobe shape with multiple profiles (ellipse 1, involute, and ellipse 2).
2. To solve the problem of the discontinuity of the curve at the boundary point for the previous type of combination (ellipse-involute), the combination is achieved by using the gradient on the boundary point according to the each profile.
3. The new design method proposed in this study eliminates the carryover phenomenon at the dedendum of the outer rotor.
4. The performance in the case of the lobe shape with multiple profiles (ellipse 1, involute, and ellipse 2) is better than that in the case of previous shapes; in particular, the flow rate and flow rate irregularity are higher and lower than those in the case of the previous shapes, respectively.

On the basis of this study, other combinations of the lobe shape with multiple profiles can be adopted, and new gerotors with various combinations can be developed by studying the dependence of the characteristics on the curve profile.

ACKNOWLEDGEMENTS

This research was financially supported by the Ministry of Education, Science Technology (MEST) and Korea Institute for Advancement of Technology (KIAT) through the Human Resource Training Project for Regional Innovation. And this work is the outcome of a Manpower Development program for Energy & Resources supported by the Ministry of Knowledge and Economy (MKE).

REFERENCES

1. Colbourne, J. R., “Gear Shape and Theoretical Flow Rate in Internal Gear Pumps,” Transactions of the CSME, Vol. 3, No. 4,

pp. 215-223, 1975.

2. Saegusa, Y., Urashima, K., Sugimoto, M., Onoda, M. and Koiso, T., "Development of Oil-Pump Rotors with a Trochoidal Tooth Shape," SAE Paper, No. 840454, 1984.
3. Tsay, C. B. and Yu, C. Y., "Mathematical Model for the Profile of Gerotor Pumps," J. CSME, Vol. 10, No. 1, pp. 41-47, 1989.
4. Yu, C. Y. and Tsay, C. B., "The Mathematical Model of Gerotor Pump Application to Its Characteristic Study," J. CSME, Vol. 11, No. 4, pp. 385-391, 1990.
5. Lee, S. C. and Lee, S. N., "Design and Analysis of Gerotor for Hydraulic Motors," Journal of KSTLE, Vol. 11, No. 2, pp. 63-70, 1995.
6. Mimmi, G. C. and Pennacchi, P. E., "Involute Gear Pumps Versus Lobe Pumps: A Comparison," J. of Mechanical Design, Vol. 119, No. 4, pp. 458-465, 1997.
7. Kim, C. H., Kim, D. I., Ahn, H. S. and Chong, T. H., "Analysis of Tooth Contact Stress of Gerotor Hydraulic Motors," J. of KSTLE, Vol. 15, No. 2, pp. 164-170, 1990.
8. Bae, J. H., Kim, M. S., Song, M. J., Jung, S. Y. and Kim, C., "A study on optimal design and fatigue life of the common rail pipe," Int. J. Precis. Eng. Manuf., Vol. 12, No. 3, pp. 475-483, 2011.
9. Kim, J. H. and Kim, C., "Development of an Integrated System of Automated Design of Gerotor Oil Pump," Journal of the KSPE, Vol. 23, No. 2, pp. 88-96, 2006.
10. Kim, J. H., Kim, C. and Chang, Y. J., "Optimum Design on Lobe Shapes of Gerotor Oil Pump," J. of Mechanical Science and Technology, Vol. 20, No. 9, pp. 1390-1398, 2006.
11. Chang, Y. J., Kim, J. H., Jeon, C. H., Kim, C. and Jung, S. Y., "Development of an Integrated System for the Automated Design of a Gerotor Oil Pump," Journal of Mechanical Design, Vol. 129, No. 10, pp. 1099-1105, 2007.
12. Colbourne, J. R., "The Geometry of Involute Gears," Springer, pp. 24-44, 1987.